Applied Catalysis B: Environmental 324 (2023) 122284

Contents lists available at ScienceDirect

Applied Catalysis B: Environmental

journal homepage: www.elsevier.com/locate/apcatb

Non-covalently linked donor-acceptor interaction enhancing photocatalytic hydrogen evolution from porphyrin assembly

Jianfang Jing [a,b], Junshan Li [c], Yiguo Su [a], Yongfa Zhu [b,*]

[a] College of Chemistry and Chemical Engineering, Inner Mongolia University, Hohhot 010021, PR China
[b] Department of Chemistry, Tsinghua University, Beijing 100084, PR China
[c] Institute for Advanced Study, Chengdu University, Chengdu 610106, PR China

ARTICLE INFO

Keywords:
Photocatalysis
Hydrogen evolution
Porphyrin
Donor-acceptor interaction

ABSTRACT

The separation of photogenerated excitons plays a crucial role in initiating high-efficiency photocatalysis of organic semiconductors. Herein, a non-covalent donor-acceptor (D-A) structure composed of tetrakis (4-carboxyphenyl) zinc porphyrin (ZnTCPP) linked to ethylenediamine functionalized fullerene (C_{60}-EDA) by electrostatic interaction was successfully developed. Due to D-A interaction, an efficient electron transfer channel from ZnTCPP to C_{60}-EDA was established, resulting in a charge-separated state with appreciable lifetime. Accordingly, the photogenerated excitons separation got considerably improved and charge-carrier exhibited faster migration to the surface of D-A assembly. ZnTCPP/C_{60}-EDA presented efficient photocatalytic H_2 evolution of 113.5 μmol h^{-1} under full spectrum, 3.9 times higher that of pure ZnTCPP. This work offers valuable insight into the non-covalent D-A construction for enhanced photocatalytic performance.

1. Introduction

Semiconductor-based photocatalytic water splitting is a promising approach for green hydrogen production, which is of great significance for addressing environmental and energy issues [1–4]. Conjugated organic materials have exhibited great potential as a viable alternative to inorganic counterparts, owing to their high earth abundance, low toxicity, broad spectrum absorption, molecular structure diversity and tunability [5,6]. Therefore, considerable effort has been invested in developing organic photocatalysts to achieve a 10% STH (solar to hydrogen) conversion efficiency. As known, porphyrins are a class of chromophores with π conjugated electrons, possessing strong light-harvesting, highly-conjugated rigid planes, tunable structure and function, and high chemical stability [7,8]. These extraordinary properties make porphyrins a versatile platform for building various photoelectric conversion materials [9–13]. In particular, porphyrin-based supramolecular materials have attracted increasing interest in photocatalytic H_2 evolution [14–17]. Tetrakis (4-carboxyphenyl) zinc porphyrin (ZnTCPP) is a promising photocatalyst for H_2 production due to strong reduction potential and high stability [14]. Unfortunately, ZnTCPP suffers from additional dissociation process of electrostatically-bound excitons, resulting in inefficient separation of photogenerated charge, which seriously hinders further development of photocatalysis [18,19]. Therefore, improving exciton separation and further enhancing the solar energy conversion efficiency of porphyrin-based photocatalysts remains a grand challenge.

Donor-acceptor (D-A) systems, which facilitate the spontaneous charge transfer from donor to acceptor, have been exercised to improve charge separation in organic photocatalysts [20]. The initial photoexcited electron-hole pairs undergo an energetically downhill electron transfer, followed by the formation of charge-separated (CS) state in the D-A system. As a result, the excitons are inhibited from falling back to the ground state for recombination, thus allowing more free charge-carrier for photocatalytic reactions [21,22]. Most of reported D-A structures are fabricated mainly by strong covalent bonds with harsh and cumbersome preparation, involving conjugated polymers, covalent organic frameworks, and D-A heterostructure [23–26]. However, few reports dedicated to rationally controlling the non-covalently linked D-A structure via facile and mild strategies to achieve efficient charge-separated states. Furthermore, the mechanism of enhancing exciton separation by modulating non-covalent interactions in D-A structure is not well understood, as most studies so far have focused only on materials development. Therefore, it is highly pursued to provide insightful analysis of exciton separation and electron migration through

* Corresponding author.
E-mail address: zhuyf@tsinghua.edu.cn (Y. Zhu).

https://doi.org/10.1016/j.apcatb.2022.122284
Received 27 October 2022; Received in revised form 7 December 2022; Accepted 9 December 2022
Available online 10 December 2022

precisely controllable non-covalent interactions in a D-A structure.

Fullerenes are preferred electron acceptors for building D-A systems because of their highly delocalized π-spherical surface, excellent electron affinity and low reorganization energy demand [27–30]. Herein, ethylenediamine functionalized fullerene (C_{60}-EDA) was adopted to integrate with ZnTCPP through simple electrostatic self-assembly to form a non-covalently linked D-A structure. The photoinduced electron transfer from ZnTCPP to C_{60}-EDA was achieved due to the well-modulated D-A interaction, resulting in a long-lived charge-separated state. Benefiting from this D-A construction, the charge separation and carrier migration of porphyrin were significantly improved, and subsequently, the photocatalytic hydrogen evolution got considerably enhanced. The optimized ZnTCPP/C_{60}-EDA assembly could achieve a hydrogen evolution rate of 113.5 μmol h^{-1}, outperforming most of the reported organic supramolecular photocatalysts.

2. Experimental section

2.1. Synthesis of C_{60}-EDA

The synthesis of ethylenediamine functionalized fullerene (C_{60}-EDA) was based on the literature with slight modifications [31]. 40 mg fullerene (C_{60}) was ultrasonically dispersed in 20 mL ethylenediamine (EDA), the mixture then was stirred at 65 °C for 12 h to form a yellow homogenous solution. Next, the solution was rotary evaporated to remove ethylenediamine, the remaining solid was dissolved in 4 M HCl HCl solution, which was rotary evaporated again, and finally obtained C_{60}-EDA solid was dissolved in water at a concentration of 2 mg mL^{-1} for further application.

2.2. Synthesis of ZnTCPP/C_{60}-EDA assembly

First, 75 mg tetrakis (4-carboxyphenyl) porphyrin (TCPP) was dissolved in 8.5 mL 0.1 M NaOH solution, then, 0.0179 g $Zn(OAc)_2$ was added and refluxed for 2 h. Cooling down to room temperature, the above ZnTCPP solution was quickly injected into 12 mM HCl solution (containing 2.5 mM CTAB), and the pH was adjusted to 2.5, followed by stirring at room temperature for 10 h. The resultants were collected by centrifugation, washed, and dried for the subsequent use. 20 mg of the resultant ZnTCPP powders were dispersed in the above prepared C_{60}-EDA solution (2 mg mL^{-1}) with different volumes. Then, the suspension was sonicated for 30 min, followed by heating and stirring at 65 °C for 8 h. The dark grey product of ZnTCPP/C_{60}-EDA assembly were collected and dried. Specifically, by adding different volumes of C_{60}-EDA solutions, the mass ratios of C_{60}-EDA to ZnTCPP in the product were 0.2, 0.4, 0.7, 1.0, 1.5, 2.0, respectively. Note that when the mass ratio of C_{60}-EDA to ZnTCPP was 1.0, the corresponding ZnTCPP/C_{60}-EDA showed the best photocatalytic H_2 evolution performance, therefore, this ZnTCPP/C_{60}-EDA was used for subsequent data characterizations in the full text.

2.3. Materials characterization

The morphologies and microstructures of the samples were investigated by transmission electron microscope (TEM) on Hitachi HT 7700 and high-resolution TEM (HRTEM). X-ray diffraction (XRD) patterns of the samples were obtained on a Bruker D8 ADVANCE X-ray diffractometer. The Fourier transform infrared (FT-IR) spectra were acquired on Bruker VERTEX 70 spectrometer. The chemical state of the samples was analyzed by X-ray photoelectron spectroscopy (XPS, PHI Quantera SXM). The optical properties of the samples were characterized by UV-Vis diffuse reflectance spectroscopy (DRS) on Agilent Cary 5000 spectrophotometer. Room temperature photoluminescence (PL) spectra were recorded on Edinburgh F900 fluorescence spectrometer with an excitation wavelength of 420 nm and emission wavelength of 677 nm. Time-resolved photoluminescence (TR-PL) spectra were collected on Edinburgh FLSP920 fluorescence spectrometer with an excitation wavelength of 420 nm and the detection wavelength is at 677 nm. The surface photovoltage (SPV) measurements were conducted with a home-built instrument as previously reported [16]. Kelvin probe force microscope (KPFM, Oxford Cypher VRS) was used to measure the surface potentials of samples in the light and dark. A 300 W Xe lamp with cut-off filter ($\lambda \geq 420$ nm) was used as the light source. The highly oriented pyrolytic graphite (HOPG) was used as substrate material on which sample suspension was spin coated. The femtosecond transient absorption spectra (TAS) were performed on a previously reported [16] home-made spectroscopic setup to illustrate kinetics of photogenerated charge separation and transfer, and the femtosecond pump excitation wavelength was 420 nm. The samples were dispersed in deionized water at a concentration of 1×10^{-5} M, and bubbled with nitrogen gas for 30 min. Electrochemical impedance spectroscopy (EIS) and Mott-Schottky plots were performed on CHI660E electrochemical workstation of Shanghai Chenhua Instrument Company. A 300 W Xe lamp with cut-off filter ($\lambda \geq 420$ nm) was used as the light source. The ITO glass (2 ×2 cm^2) deposited with sample slurry offered the working electrode, the Pt wire and saturated calomel electrode were used as counter electrode and reference electrode, respectively. 0.1 M Na_2SO_4 was used as electrolyte solution.

2.4. Photocatalytic hydrogen evolution experiments

The photocatalytic hydrogen evolution test was performed on Labsolar-6A water splitting system provided by Beijing Perfectlight (Fig. S1). Typically, 7 mg photocatalyst powders were dispersed in 100 mL distilled water with 0.2 M ascorbic acid as sacrificial agent. 5 wt% Pt as co-catalyst was loaded on the photocatalysts by in-situ photo-deposition method using H_2PtCl_6. Then, the suspension was thoroughly degassed and irradiated using a 300 W Xe lamp (without filter, light intensity 632 mW cm^{-2}) or with a cut-off filter ($\lambda \geq 420$ nm, light intensity 445 mW cm^{-2}). The evolved gases were analyzed at 30 min interval by an online gas chromatograph (GC-2002 N/TFF, TCD detector, Ar carrier, 5 Å molecular sieve column). The apparent quantum efficiency (AQE) of photocatalytic hydrogen evolution was measured with different band-pass filters of 400, 420, 450, 500, 550, 600, and 650 nm. The AQE was calculated as following equation:

$$\mathrm{AQE}(\%) = \frac{\text{the number of evolved } H_2 \text{ molecules} \times 2}{\text{number of incident } photons} \times 100\%$$

2.5. Theoretical computational method

Theoretical calculations were carried out through Density Functional Theory (DFT) with Gaussian 09 software. B3LYP/6–31 G(d,p) (Lanl2dz pseudopotential for metal) method was used for molecular optimization. M062x/6–311 + +G(2df,2p) (Lanl2dz pseudopotential for metal) method was used for single-point energy calculations. The highest occupied molecular orbital (HOMO), lowest unoccupied molecular orbital (LUMO) and electrostatic potential distribution were analyzed and drawn using Multiwfn program [32] and VMD software [33].

3. Results and discussion

3.1. Construction of ZnTCPP/C_{60}-EDA assembly with D-A structure

EDA moieties are easily modified onto fullerenes by nucleophilic addition according to the previous report [31] (Fig. S2). In the presence of multiple amino motifs in fullerenes, C_{60}-EDA can be easily protonated by HCl to make its surface positively charged. As observed in Zeta potential measurements (Fig. 1a, Table S1), the Zeta potential of C_{60}-EDA is + 29.9 mV, while ZnTCPP presents a negatively charged surface, with the zeta potential of − 60.3 mV. In this case, a ZnTCPP/C_{60}-EDA assembly with D-A structure was constructed by electrostatic interaction (Fig. S3). Electrostatic potential distribution clearly depicts this strong

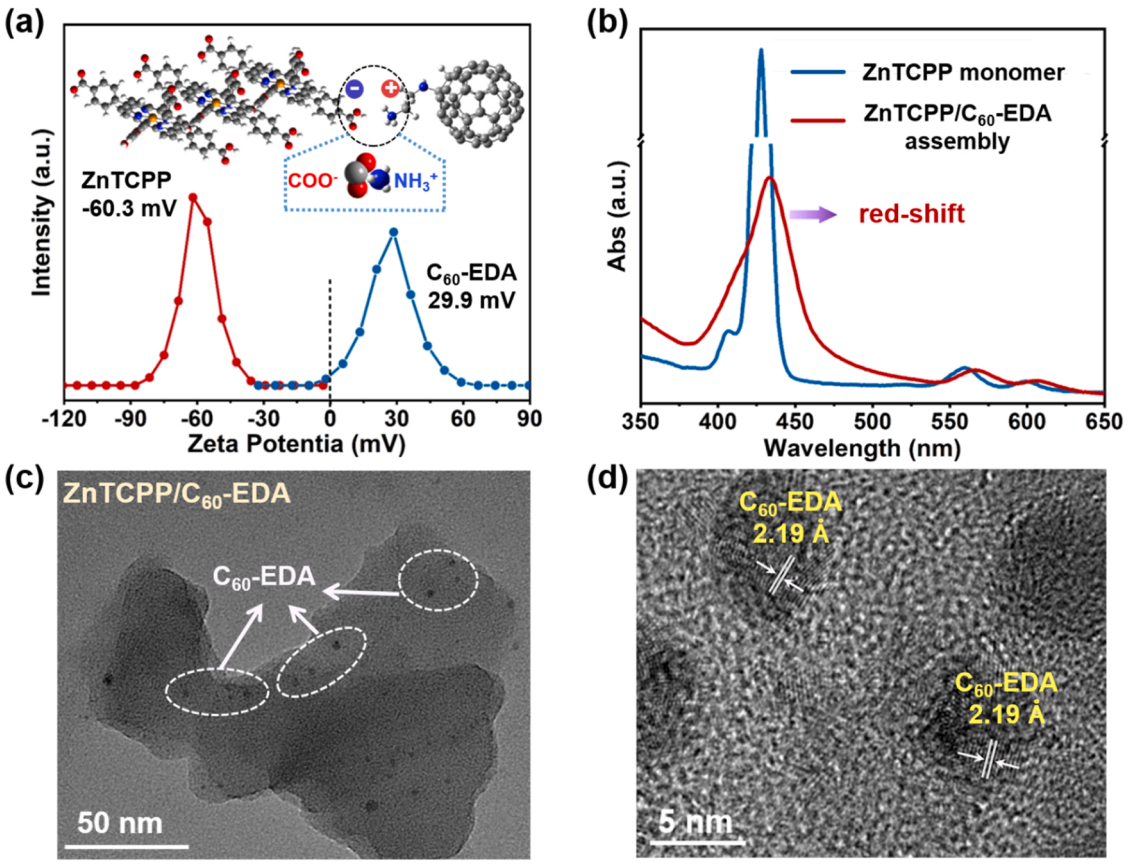

Fig. 1. Construction of D-A assembly by electrostatic interaction. (a) Zeta potential of ZnTCPP and protonated C_{60}-EDA dispersed in deionized water at pH 7. (b) UV-Vis absorption spectroscopy. (c) TEM image of ZnTCPP/C_{60}-EDA. (d) HRTEM image of ZnTCPP/C_{60}-EDA.

electrostatic interaction between carboxyl groups and protonated amino motifs (Fig. S4). Futhermore, the HOMO distributed in porphyrin moiety and the LUMO distributed in C_{60}-EDA moiety directly demonstrate the D-A characteristic [34,35], with ZnTCPP and C_{60}-EDA units acting as electron donor and acceptor, respectively (Fig. S5). In order to further confirm the successful construction of D-A assembly, Fourier transform infrared (FT-IR) spectra and X-ray photoelectron spectroscopy (XPS) were analyzed for the prepared sample. Compared to pure ZnTCPP, the IR characteristic peaks of carbonyl in D-A assembly significantly shift to lower wavenumber of 1601 cm^{-1} and 1502 cm^{-1}, indicating that the strong electrostatic attraction contributes to the conjugation of carbonyl with nitrogen atom (Fig. S6a). Besides, the C-O peak of O1s in XPS is observed at higher binding energy of 531.6 eV, suggesting the electron transfer from ZnTCPP to C_{60}-EDA due to electrostatic interaction (Fig. S6b) [10]. The two peaks of Zn $2p_{1/2}$ and Zn $2p_{3/2}$ were unchanged in the D-A structure (Fig. S6c), indicating that no coordination occurred between Zn and ethylenediamine. Furthermore, UV-Vis absorption spectra were employed to reveal the assembly pattern of the D-A structure. ZnTCPP/C_{60}-EDA assembly exhibits a broader absorption band, simultaneously accompanied by red-shift compared to the ZnTCPP monomer (Fig. 1b), indicating the J-type aggregation [36]. As the C_{60}-EDA component increases, the Soret band of ZnTCPP shows an increasing red-shift trend (Fig. S6d), proving that the electrostatic interaction between ZnTCPP and C_{60}-EDA enhances the electron delocalization and decreases transition energy [37].

Transmission electron microscopy (TEM) image gives morphology information for the D-A assembly. Tiny C_{60}-EDA particles within 10 nm are clearly observed distributed on the surface of ZnTCPP nanosheets (Fig. 1c, Fig. S7), indirectly confirming the occurrence of electrostatic interaction between ZnTCPP and C_{60}-EDA, leading to the successful formation of D-A assembly. High resolution transmission electron microscope (HRTEM) observation for ZnTCPP/C_{60}-EDA indicates that lots of lattice fringes of 2.19 Å are attributed to C_{60}-EDA (Fig. 1d, Fig. S8-9), this high crystallinity is favorable for long-distance electron transport.

3.2. Electron transfer mechanism by D-A interaction

In order to elaborate on charge separation mechanism and electron transfer dynamics in D-A structure, the transient absorption spectra (TAS) measurements were performed under femtosecond pump excitation at 420 nm (Fig. S10). As shown in Fig. 2a, both ZnTCPP and ZnTCPP/C_{60}-EDA exhibits a strong ground state bleaching (GSB) at 400–450 nm, which corresponds to the Soret band absorption (S_0-S_2). For ZnTCPP, the excited state absorption (ESA) with a maximum at 457 nm is attributed to transition of triplet state (*ZnTCPP^3) originating from S_2 excited state [38,39]. When assembled as the D-A structure, this ESA peak obviously shifts to 542 nm. Then, the decay profiles of transient absorbance at 457 nm for ZnTCPP and at 542 nm for ZnTCPP/C_{60}-EDA were fitted with a two-exponential function, respectively (Fig. S11). As depicted in Fig. 2b, ZnTCPP/C_{60}-EDA exhibits significantly reduced time constants τ_1 and τ_2, indicating that *ZnTCPP^3 is effectively reduced due to the strong D-A interaction of porphyrin with C_{60}-EDA [40,41]. That is, electrons transfer from *ZnTCPP^3 to C_{60}-EDA, possibly followed by the production of CS state. The ESA peaks in the range of 570–700 nm correspond to intermediates formed by electron transfer or ZnTCPP$^{\bullet+}$ [41,42], and the decay kinetic profiles collected at 640 nm were used as representative data for analysis (Fig. 2c, Fig. S11). Apparently, the τ_1 (22.2 ps) of ZnTCPP$^{\bullet+}$ for ZnTCPP/C_{60}-EDA is dramatically prolonged to 4.8 times that of pure ZnTCPP (τ_1 = 4.6 ps), while the τ_2 is almost the same, which would be conducive to the formation of the CS state. The CS state was detected by near-infrared

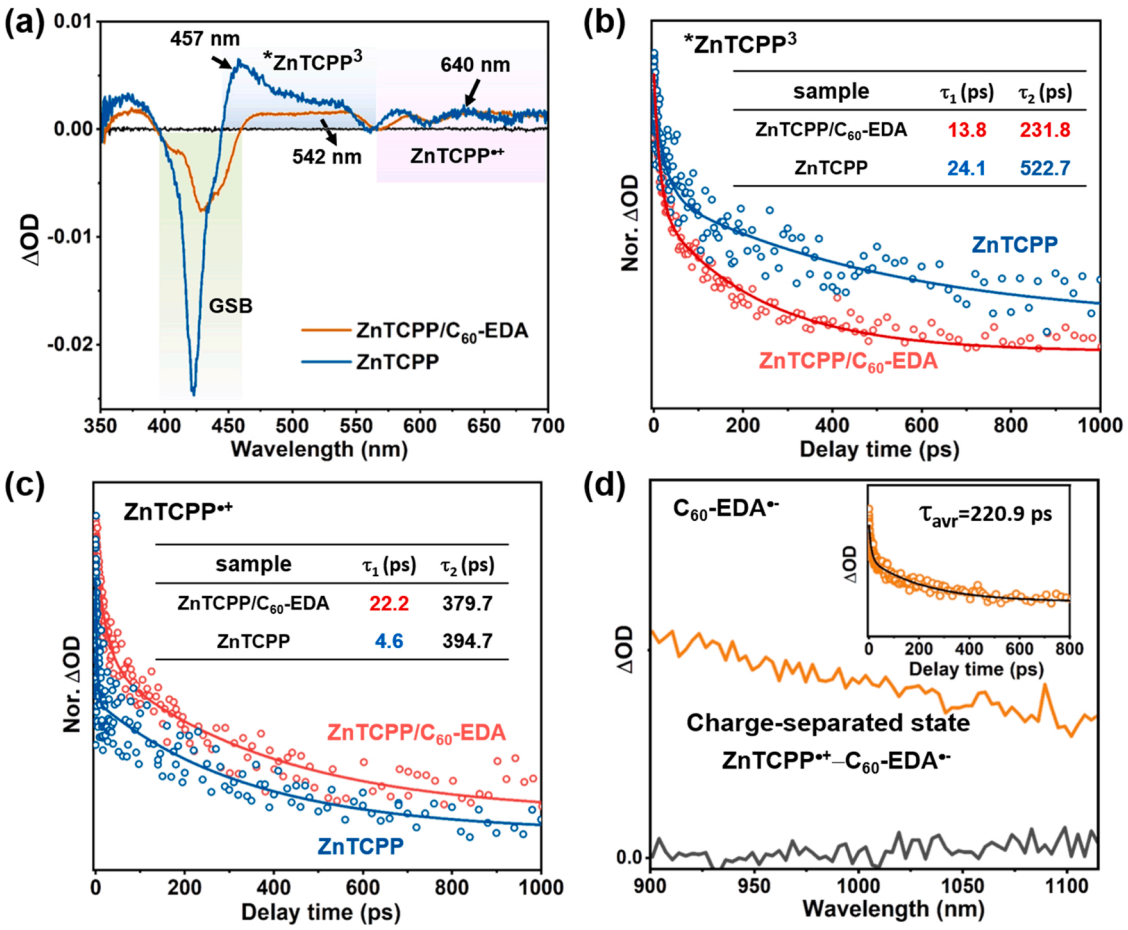

Fig. 2. Electron transfer route and charge-separated state formation. (a) Transient absorption spectra (TAS). The decay kinetics of (b) *ZnTCPP^3 and (c) ZnTCPP$^{\bullet+}$ fitted with two-exponential function, the inset table shows fitting results. (d) NIR TAS of ZnTCPP/C_{60}-EDA and decay kinetics probed at 1000 nm (Inset).

transient absorption, the absorption band near 1000 nm for ZnTCPP/C_{60}-EDA agrees with fullerene radical anion (C_{60}-EDA$^{\bullet-}$) [43] (Fig. 2d, Fig. S12). This observation clearly confirms that electrons transfer from ZnTCPP* to C_{60}-EDA, forming the CS state (ZnTCPP$^{\bullet+}$-C_{60}-EDA$^{\bullet-}$) [44,45]. Given the kinetic profiles probed at 1000 nm, the lifetime (τ_{avr} = 220.9 ps) of CS state for ZnTCPP/C_{60}-EDA is remarkably elongated (Fig. S13), demonstrating that the non-covalently linked D-A interaction definitely enables the generation of long-lived CS state.

The above TAS results elucidate that D-A assembly enables efficient electron transfer from ZnTCPP to C_{60}-EDA and the formation of CS state, which would evidently boost the separation of photogenerated excitons into free charge-carrier. The migration efficiency of charge-carrier to the photocatalyst surface also restricts the photocatalytic performance. Therefore, the charge-carrier migration properties of D-A assembly were investigated by photophysical and electrochemical characterizations.

3.3. *Efficient charge-carrier migration of ZnTCPP/C_{60}-EDA*

As shown in Fig. 3a, ZnTCPP/C_{60}-EDA exhibits almost all negative surface photovoltage (SPV) signals, demonstrating that under irradiation, photogenerated electrons from ZnTCPP transfer to the surface of catalysts as the dominant charge-carrier [15]. Meanwhile, the SPV response is significantly enhanced, implying higher carrier migration efficiency [46]. The carrier migration was also reflected by photoluminescence (PL) spectrum. The intensity of fluorescence emission peak (677 nm) is remarkably decreased on ZnTCPP/C_{60}-EDA (Fig. 3b), suggesting that the carrier recombination is effectively suppressed, thus improving the utilization of photogenerated charge. Moreover, the time-resolved fluorescence spectrum at the corresponding steady-state emission peak was measured. ZnTCPP/C_{60}-EDA features a longer average lifetime (τ_A) of charge-carrier (Inset in Fig. 3b, Table S2), indicating the longer diffusive migration distance of photogenerated carriers and reduced non-radiative recombination [47]. To further gain direct evidence of efficient carrier migration, Kelvin probe force microscopy (KPFM) measurements were analyzed. As seen in Fig. 3c, the surface potential for two samples are both enhanced under irradiation compared to the dark condition. ZnTCPP/C_{60}-EDA significantly increases by 16 mV, while ZnTCPP only increases by 5 mV (Fig. S14-15), confirming that more photogenerated carriers migrate to the surface of ZnTCPP/C_{60}-EDA under illumination [48,49], which is consistent with the results obtained by SPV and PL. In addition, the electrochemical impedance spectra (EIS) displays the fitted charge transfer resistance (R_{ct}) of ZnTCPP/C_{60}-EDA is much lower than that of ZnTCPP (Fig. 3d, Table S3), indicating the faster migration of photogenerated carriers on D-A assembly.

3.4. *Hydrogen production performance*

All the experimental results identically confirm that ZnTCPP/C_{60}-EDA has highly efficient charge separation and carrier migration, and accordingly, the photocatalytic activity of ZnTCPP/C_{60}-EDA would be enhanced. Before the evaluation of photocatalytic activity, the band structure of D-A assembly was investigated (Fig. S16-**17**). ZnTCPP/C_{60}-EDA exhibits a wide solar spectrum absorption, with the intrinsic absorption band edge reaching 710 nm. The conduction band position is determined to be − 1.10 V (vs. NHE, pH=7), which is more negative than the H^+/H_2 redox potential (−0.41 V vs. NHE, pH=7). These results

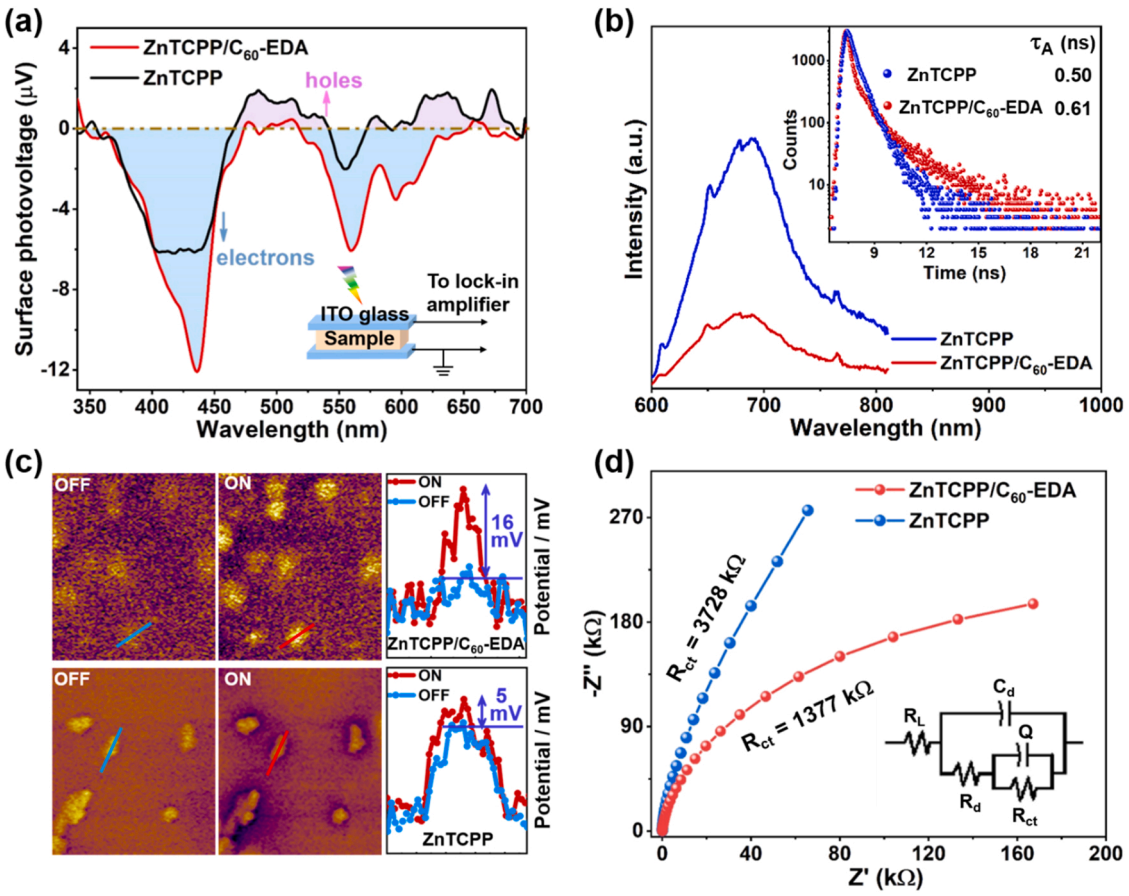

Fig. 3. Efficient charge-carrier migration. (a) SPV spectra, Inset: schematic setup for the SPV measurement. (b) PL spectrum, Inset: time-resolved transient PL spectrum. (c) Surface potential images measured with KPFM, ON: under irradiation; OFF: in the dark, (d) EIS results, Inset: equivalent circuit of the model.

illustrate that ZnTCPP/C_{60}-EDA has favorable thermodynamic driving force for photocatalytic H_2 evolution.

Subsequently, the photocatalytic H_2 evolution using sacrificial reagent was measured under full-spectrum (300–800 nm) irradiation. The H_2 evolution rate of ZnTCPP/C_{60}-EDA can reach 113.5 μmol h^{-1} (≈16.2 mmol h^{-1} g^{-1}), with optimal catalyst dosage (7 mg) and co-catalyst loading amount (5 wt% Pt) (Fig. 4a, Fig. S18-19). Compared with pristine ZnTCPP under the same test conditions, the H_2 evolution activity of ZnTCPP/C_{60}-EDA is improved by 3.9 times, and such an extraordinary activity is simultaneously higher than that of the most reported supramolecular materials. (Table S4). Meanwhile, ZnTCPP/C_{60}-EDA possesses excellent visible light-driven H_2 evolution of 88.4 μmol h^{-1}, and achieves the H_2 evolution of 44.2 μmol h^{-1} under long-wavelength light irradiation (λ > 550 nm) (Fig. 4b, Fig. S20), confirming its wide-spectrum response for photocatalysis. The performance of 23.5 μmol h^{-1} was detected under simulated sunlight irradiation (AM 1.5 G, 100 mW cm^{-2}), further indicating an efficient solar-to-hydrogen energy conversion of ZnTCPP/C_{60}-EDA. The AQE of 0.78% at 420 nm is obtained, which is 5.7 times higher than that of the supramolecular ZnTCPP (0.138%) in previous work (Fig. 4c, Table S5) [14]. Additionally, the identical trend between AQE values and optical absorption spectrum is observed in Fig. 4c, meaning that the photocatalytic reaction of ZnTCPP/C_{60}-EDA is driven by absorbing incident photons, and the H_2 evolution experiments at single wavelength also give a similar result (Fig. S21). Satisfactorily, TEM, UV-Vis DRS, IR, XRD and XPS characteristics of the recovered catalyst after 10 cycle tests are almost unchanged (Fig. S22-23), suggesting a high stability of ZnTCPP/C_{60}-EDA, consequently, no noticeable decrease of H_2 evolution activity occurs during the long-term photocatalytic reaction (Fig. 4d).

According to the above analysis, the mechanism of enhanced photocatalytic H_2 evolution performance of D-A assembly can be illustrated in Fig. 5. The photogenerated excitons are generated inside ZnTCPP under light excitation, and electrons transfer from ZnTCPP to C_{60}-EDA through D-A interaction linked by electrostatic self-assembly. Therefore, the charge separation of ZnTCPP gets considerably improved, and more photogenerated electrons migrate to the surface of catalyst for H_2 production reaction with the help of co-catalyst Pt. Consequently, the D-A assembly ZnTCPP/C_{60}-EDA exhibits an outstanding H_2 evolution rate of 113.5 μmol h^{-1}.

4. Conclusions

In conclusion, the modified fullerene was integrated with zinc porphyrin through electrostatic self-assembly to successfully construct a ZnTCPP/C_{60}-EDA photocatalyst with D-A characteristic. The efficient electron transfer from ZnTCPP to C_{60}-EDA was achieved, resulting in a long-lived charge-separated state in D-A assembly, which significantly facilitated photogenerated excitons separation. Meanwhile, ZnTCPP/C_{60}-EDA presented fast charge-carrier migration to the catalyst surface. As a result, the photocatalytic H_2 evolution of ZnTCPP/C_{60}-EDA reached 113.5 μmol h^{-1} under full spectrum, increased to 3.9 times that of the pristine porphyrin. This work not only provided a feasible strategy to design high-performance D-A photocatalysts, but also promoted better understanding of the mechanism in enhanced charge separation of organic photocatalysts.

CRediT authorship contribution statement

Jianfang Jing: Design, Validation, Methodology, Experiments, Data analysis, Writing – original draft, Writing – review & editing, **Junshan**

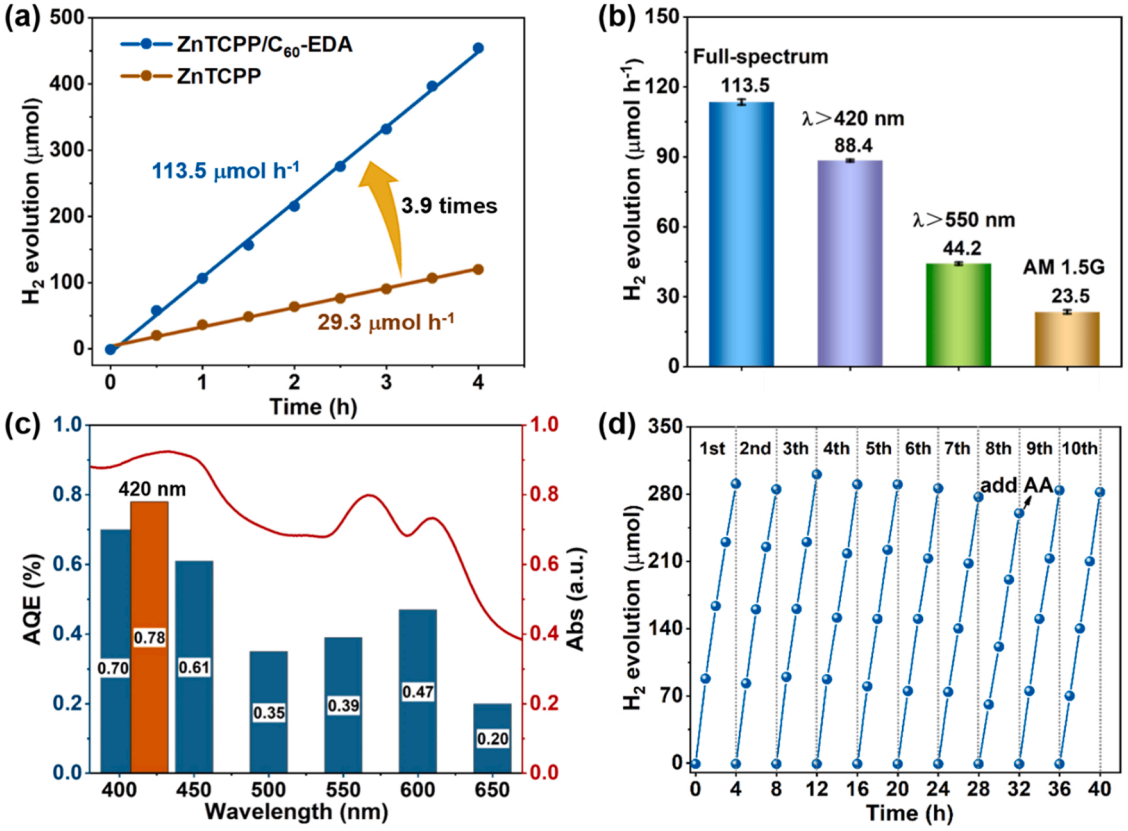

Fig. 4. Efficient photocatalytic hydrogen evolution. (a) H_2 evolution under full-spectrum irradiation (300–800 nm, Light intensity is 632 mW cm^{-2}), Reaction conditions: 7 mg photocatalyst, 5 wt% Pt as co-catalyst and 0.2 M ascorbic acid (AA) as sacrificial reagent. (b) H_2 evolution tests under incident light with varied wavelengths. (c) The wavelength-dependent AQE and UV-Vis DRS spectrum. (d) The repeated cycles of photocatalytic H_2 evolution.

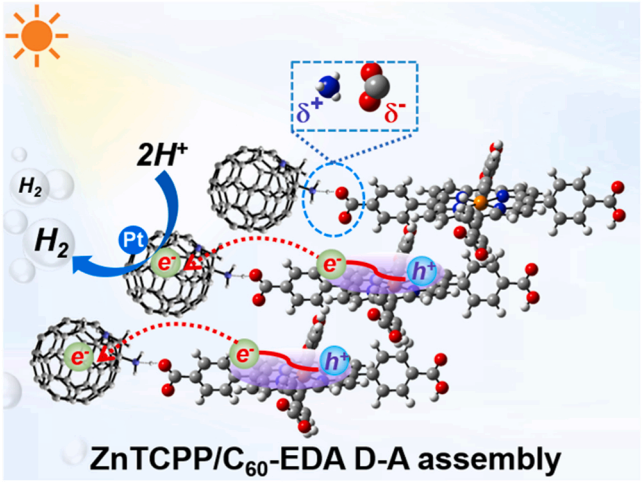

Fig. 5. Schematic mechanism of photocatalytic H_2 evolution for ZnTCPP/C_{60}-EDA.

Li: Visualization, Investigation, **Yiguo Su**: Visualization, Writing – review, **Yongfa Zhu**: Overall supervision, Resources, Writing – review & editing.

Declaration of Competing Interest

The authors declare that they have no known competing financial interests or personal relationships that could have appeared to influence the work reported in this paper.

Data Availability

No data was used for the research described in the article.

Acknowledgements

We are grateful for the financial grants from National Natural Science Foundation of China (22136002, 21872077, 21621003), National Key Research and Development Project of China (2020YFA0710304).

Appendix A. Supporting information

Supplementary data associated with this article can be found in the online version at doi:10.1016/j.apcatb.2022.122284.

References

[1] X. Chen, S. Shen, L. Guo, S.S. Mao, Semiconductor-based photocatalytic hydrogen generation, Chem. Rev. 110 (2010) 6503–6570, https://doi.org/10.1021/cr1001645.
[2] H. Li, H. Gong, Z. Jin, Phosphorus modified Ni-MOF–74/$BiVO_4$ S-scheme heterojunction for enhanced photocatalytic hydrogen evolution, Appl. Catal. B Environ. 307 (2022), 121166, https://doi.org/10.1016/j.apcatb.2022.121166.
[3] H. Gong, Y. Li, H. Li, Z. Jin, 2D CeO_2 and a partially phosphated 2D Ni-based metal-organic framework formed an S-Scheme heterojunction for efficient photocatalytic hydrogen evolution, Langmuir 38 (2022) 2117–2131, https://doi.org/10.1021/acs.langmuir.1c03198.
[4] T. Li, Y. Li, Z. Jin, Surface-induced engineering: P-induced formation of surface bonding states based on the ZIF synthesis strategy for photocatalytic hydrogen evolution, Inorg. Chem. 61 (2022) 12809–12821, https://doi.org/10.1021/acs.inorgchem.2c01909.
[5] C. Zhao, Z. Chen, R. Shi, X. Yang, T. Zhang, Recent advances in conjugated polymers for visible-light-driven water splitting, Adv. Mater. 32 (2020) 1907296, https://doi.org/10.1002/adma.201907296.

[6] Q. Yang, M. Luo, K. Liu, H. Cao, H. Yan, Covalent organic frameworks for photocatalytic applications, Appl. Catal. B Environ. 276 (2020), 119174, https://doi.org/10.1016/j.apcatb.2020.119174.

[7] K. Gao, Y. Kan, X. Chen, F. Liu, B. Kan, L. Nian, X. Wan, Y. Chen, X. Peng, T. P. Russell, Y. Cao, A.K.Y. Jen, Low-bandgap porphyrins for highly efficient organic solar cells: materials, morphology, and applications, Adv. Mater. 32 (2020) 1906129, https://doi.org/10.1002/adma.201906129.

[8] W. Ji, T.-X. Wang, X. Ding, S. Lei, B.-H. Han, Porphyrin- and phthalocyanine-based porous organic polymers: from synthesis to application, Coord. Chem. Rev. 439 (2021), 213875, https://doi.org/10.1016/j.ccr.2021.213875.

[9] Q. Yin, E.V. Alexandrov, D.-H. Si, Q.-Q. Huang, Z.-B. Fang, Y. Zhang, A.-A. Zhang, W.-K. Qin, Y.-L. Li, T.-F. Liu, D.M. Proserpio, Metallization-prompted robust porphyrin-based hydrogen-bonded organic frameworks for photocatalytic CO_2 reduction, e202115854, Angew. Chem. Int. Ed. 61 (2022), https://doi.org/10.1002/anie.202115854.

[10] E.S. Da Silva, N.M.M. Moura, M.G.P.M.S. Neves, A. Coutinho, M. Prieto, C.G. Silva, J.L. Faria, Novel hybrids of graphitic carbon nitride sensitized with free-base meso-tetrakis(carboxyphenyl) porphyrins for efficient visible light photocatalytic hydrogen production, Appl. Catal. B Environ. 221 (2018) 56–69, https://doi.org/10.1016/j.apcatb.2017.08.079.

[11] H. Hu, Z. Wang, L. Cao, L. Zeng, C. Zhang, W. Lin, C. Wang, Metal-organic frameworks embedded in a liposome facilitate overall photocatalytic water splitting, Nat. Chem. 13 (2021) 358–366, https://doi.org/10.1038/s41557-020-00635-5.

[12] Z.-B. Fang, T.-T. Liu, J. Liu, S. Jin, X.-P. Wu, X.-Q. Gong, K. Wang, Q. Yin, T.-F. Liu, R. Cao, H.-C. Zhou, Boosting interfacial charge-transfer kinetics for efficient overall CO_2 photoreduction via rational design of coordination spheres on metal-organic frameworks, J. Am. Chem. Soc. 142 (2020) 12515–12523, https://doi.org/10.1021/jacs.0c05530.

[13] Q. Zuo, T. Liu, C. Chen, Y. Ji, X. Gong, Y. Mai, Y. Zhou, Ultrathin metal-organic framework nanosheets with ultrahigh loading of single Pt atoms for efficient visible-light-driven photocatalytic H_2 evolution, Angew. Chem. Int. Ed. 58 (2019) 10198–10203, https://doi.org/10.1002/anie.201904058.

[14] J. Jing, J. Yang, Z. Zhang, Y. Zhu, Supramolecular zinc porphyrin photocatalyst with strong reduction ability and robust built-in electric field for highly efficient hydrogen production, Adv. Energy Mater. 11 (2021) 2101392, https://doi.org/10.1002/aenm.202101392.

[15] Z. Zhang, Y. Zhu, X. Chen, H. Zhang, J. Wang, A full-spectrum metal-free porphyrin supramolecular photocatalyst for dual functions of highly efficient hydrogen and oxygen evolution, Adv. Mater. 31 (2019) 1806626, https://doi.org/10.1002/adma.201806626.

[16] J. Jing, J. Yang, W. Li, Z. Wu, Y. Zhu, Construction of interfacial electric field via dual-porphyrin heterostructure boosting photocatalytic hydrogen evolution, Adv. Mater. 34 (2022) 2106807, https://doi.org/10.1002/adma.202106807.

[17] J. Yang, J. Jing, W. Li, Y. Zhu, Electron donor-acceptor interface of TPPS/PDI boosting charge transfer for efficient photocatalytic hydrogen evolution, Adv. Sci. 9 (2022) 2201134, https://doi.org/10.1002/advs.202201134.

[18] F. Le Formal, S.R. Pendlebury, M. Cornuz, S.D. Tilley, M. Grätzel, J.R. Durrant, Back electron-hole recombination in hematite photoanodes for water splitting, J. Am. Chem. Soc. 136 (2014) 2564–2574, https://doi.org/10.1021/ja412058x.

[19] M. Rahman, H. Tian, T. Edvinsson, Revisiting the limiting factors for overall water-splitting on organic photocatalysts, Angew. Chem. Int. Ed. 59 (2020) 16278–16293, https://doi.org/10.1002/anie.202002561.

[20] S. Bi, Z.-A. Lan, S. Paasch, W. Zhang, Y. He, C. Zhang, F. Liu, D. Wu, X. Zhuang, E. Brunner, X. Wang, F. Zhang, Substantial cyano-substituted fully sp^2-carbon-linked framework: metal-free approach and visible-light-driven hydrogen evolution, Adv. Funct. Mater. 27 (2017) 1703146, https://doi.org/10.1002/adfm.201703146.

[21] T.M. Clarke, J.R. Durrant, Charge photogeneration in organic solar cells, Chem. Rev. 110 (2010) 6736–6767, https://doi.org/10.1021/cr900271s.

[22] T.M. Clarke, A. Ballantyne, S. Shoaee, Y.W. Soon, W. Duffy, M. Heeney, I. McCulloch, J. Nelson, J.R. Durrant, Analysis of charge photogeneration as a key determinant of photocurrent density in polymer: fullerene solar cells, Adv. Mater. 22 (2010) 5287–5291, https://doi.org/10.1002/adma.201002357.

[23] H. Che, C. Liu, G. Che, G. Liao, H. Dong, C. Li, N. Song, C. Li, Facile construction of porous intramolecular g-C_3N_4-based donor-acceptor conjugated copolymers as highly efficient photocatalysts for superior H_2 evolution, Nano Energy 67 (2020), 104273, https://doi.org/10.1016/j.nanoen.2019.104273.

[24] Z.-A. Lan, W. Ren, X. Chen, Y. Zhang, X. Wang, Conjugated donor-acceptor polymer photocatalysts with electron-output "tentacles" for efficient hydrogen evolution, Appl. Catal. B Environ. 245 (2019) 596–603, https://doi.org/10.1016/j.apcatb.2019.01.010.

[25] F. Yu, Z. Wang, S. Zhang, H. Ye, K. Kong, X. Gong, J. Hua, H. Tian, Molecular engineering of donor-acceptor conjugated polymer/g-C_3N_4 heterostructures for significantly enhanced hydrogen evolution under visible-light irradiation, Adv. Funct. Mater. 28 (2018) 1804512, https://doi.org/10.1002/adfm.201804512.

[26] W. Li, X. Huang, T. Zeng, Y.A. Liu, W. Hu, H. Yang, Y.-B. Zhang, K. Wen, Thiazolo[5,4-d]thiazole-based donor-acceptor covalent organic framework for sunlight-driven hydrogen evolution, Angew. Chem. Int. Ed. 60 (2021) 1869–1874, https://doi.org/10.1002/anie.202014408.

[27] J. Zhang, J. Tan, Z. Ma, W. Xu, G. Zhao, H. Geng, Ca Di, W. Hu, Z. Shuai, K. Singh, D. Zhu, Fullerene/sulfur-bridged annulene cocrystals: two-dimensional segregated heterojunctions with ambipolar transport properties and photoresponsivity, J. Am. Chem. Soc. 135 (2013) 558–561, https://doi.org/10.1021/ja310098k.

[28] B. Park, S.E. Cho, Y. Kim, W.J. Lee, N.-H. You, I. In, E. Reichmanis, Simultaneous study of exciton diffusion/dissociation and charge transport in a donor-acceptor bilayer: pentacene on a C_{60}-terminated self-assembled monolayer, Adv. Mater. 25 (2013) 6453–6458, https://doi.org/10.1002/adma.201302934.

[29] I. Hiroshi, H. Kiyoshi, A. Tsuyoshi, A. Masanori, T. Seiji, O. Tadashi, S. Masahiro, S. Yoshiteru, The small reorganization energy of C_{60} in electron transfer, Chem. Phys. Lett. 263 (1996) 545–550, https://doi.org/10.1016/S0009-2614(96)01244-4.

[30] A. Takai, M. Chkounda, A. Eggenspiller, C.P. Gros, M. Lachkar, J.-M. Barbe, S. Fukuzumi, Efficient photoinduced electron transfer in a porphyrin tripod-fullerene supramolecular complex via π-π interactions in nonpolar media, J. Am. Chem. Soc. 132 (2010) 4477–4489, https://doi.org/10.1021/ja100192x.

[31] J. Li, F. Zhao, T. Wang, M. Nie, J. Li, Z. Wei, L. Jiang, C. Wang, Ethylenediamine functionalized fullerene nanoparticles as independent electron transport layers for high-efficiency inverted polymer solar cells, J. Mater. Chem. A 5 (2017) 947–951, https://doi.org/10.1039/C6TA09173C.

[32] T. Lu, F. Chen, Multiwfn: a multifunctional wavefunction analyzer, J. Comput. Chem. 33 (2012) 580–592, https://doi.org/10.1002/jcc.22885.

[33] W. Humphrey, A. Dalke, K. Schulten, VMD: visual molecular dynamics, J. Mol. Graph 14 (1996) 33–38, https://doi.org/10.1016/0263-7855(96)00018-5.

[34] K. Wang, C.-J. Zheng, W. Liu, K. Liang, Y.-Z. Shi, S.-L. Tao, C.-S. Lee, X.-M. Ou, X.-H. Zhang, Avoiding energy loss on TADF emitters: controlling the dual conformations of D-A structure molecules based on the pseudoplanar segments, Adv. Mater. 29 (2017) 1701476, https://doi.org/10.1002/adma.201701476.

[35] Y. Liu, Z. Liao, X. Ma, Z. Xiang, Ultrastable and efficient visible-light-driven hydrogen production based on donor-acceptor copolymerized covalent organic polymer, ACS Appl. Mater. Interfaces 10 (2018) 30698–30705, https://doi.org/10.1021/acsami.8b10022.

[36] S. Mandal, S.K. Nayak, S. Mallampalli, A. Patra, Surfactant-assisted porphyrin based hierarchical nano/micro assemblies and their efficient photocatalytic behavior, ACS Appl. Mater. Interfaces 6 (2014) 130–136, https://doi.org/10.1021/am403518d.

[37] F. D'Souza, O. Ito, Supramolecular donor-acceptor hybrids of porphyrins/phthalocyanines with fullerenes/carbon nanotubes: electron transfer, sensing, switching, and catalytic applications, Chem. Commun. 33 (2009) 4913–4928, https://doi.org/10.1039/B905753F.

[38] E. Giannoudis, E. Benazzi, J. Karlsson, G. Copley, S. Panagiotakis, G. Landrou, P. Angaridis, V. Nikolaou, C. Matthaiaki, G. Charalambidis, E.A. Gibson, A. G. Coutsolelos, Photosensitizers for H_2 evolution based on charged or neutral Zn and Sn porphyrins, Inorg. Chem. 59 (2020) 1611–1621, https://doi.org/10.1021/acs.inorgchem.9b01838.

[39] K. Peuntinger, T. Lazarides, D. Dafnomili, G. Charalambidis, G. Landrou, A. Kahnt, R.P. Sabatini, D.W. McCamant, D.T. Gryko, A.G. Coutsolelos, D.M. Guldi, Photoinduced charge transfer in porphyrin-cobaloxime and corrole-cobaloxime hybrids, J. Phys. Chem. C 117 (2013) 1647–1655, https://doi.org/10.1021/jp311766s.

[40] T. Lazarides, M. Delor, I.V. Sazanovich, T.M. McCormick, I. Georgakaki, G. Charalambidis, J.A. Weinstein, A.G. Coutsolelos, Photocatalytic hydrogen production from a noble metal free system based on a water soluble porphyrin derivative and a cobaloxime catalyst, Chem. Commun. 50 (2014) 521–523, https://doi.org/10.1039/C3CC45025B.

[41] E. Nikoloudakis, M. Pigiaki, M.N. Polychronaki, A. Margaritopoulou, G. Charalambidis, E. Serpetzoglou, A. Mitraki, P.A. Loukakos, A.G. Coutsolelos, Self-assembly of porphyrin dipeptide conjugates toward hydrogen production, ACS Sustain. Chem. Eng. 9 (2021) 7781–7791, https://doi.org/10.1021/acssuschemeng.1c00978.

[42] J. Fajer, D.C. Borg, A. Forman, D. Dolphin, R.H. Felton, pi.-cation radicals and dications of metalloporphyrins, J. Am. Chem. Soc. 92 (1970) 3451–3459, https://doi.org/10.1021/ja00714a038.

[43] C.O.O. Gary, N. Lim, Prof. Dr. Francis D'Souza, A high-energy charge-separated state of 1.70 eV from a high-potential donor-acceptor dyad: a catalyst for energy-demanding photochemical reactions, Angew. Chem. Int. Ed. 55 (2016) 11517–11521, https://doi.org/10.1002/anie.201606112.

[44] K. Ohkubo, H. Kotani, J. Shao, Z. Ou, K.M. Kadish, G. Li, R.K. Pandey, M. Fujitsuka, O. Ito, H. Imahori, S. Fukuzumi, Production of an ultra-long-lived charge-separated state in a zinc chlorin-C_{60} dyad by one-step photoinduced electron transfer, Angew. Chem. Int. Ed. 43 (2004) 853–856, https://doi.org/10.1002/anie.200352870.

[45] X. Yu, B. Wang, Y. Kim, J. Park, S. Ghosh, B. Dhara, R.D. Mukhopadhyay, J. Koo, I. Kim, S. Kim, I.-C. Hwang, S. Seki, D.M. Guldi, M.-H. Baik, K. Kim, Supramolecular fullerene tetramers concocted with porphyrin boxes enable efficient charge separation and delocalization, J. Am. Chem. Soc. 142 (2020) 12596–12601, https://doi.org/10.1021/jacs.0c05339.

[46] X. Chen, J. Wang, Y. Chai, Z. Zhang, Y. Zhu, Efficient photocatalytic overall water splitting induced by the giant internal electric field of a g-C_3N_4/rGO/PDIP Z-scheme heterojunction, Adv. Mater. 33 (2021) 2007479, https://doi.org/10.1002/adma.202007479.

[47] M. Hao, Y. Bai, S. Zeiske, L. Ren, J. Liu, Y. Yuan, N. Zarrabi, N. Cheng, M. Ghasemi, P. Chen, M. Lyu, D. He, J.-H. Yun, Y. Du, Y. Wang, S. Ding, A. Armin, P. Meredith, G. Liu, H.-M. Cheng, L. Wang, Ligand-assisted cation-exchange engineering for high-efficiency colloidal $Cs_{1-x}FA_xPbI_3$ quantum dot solar cells with reduced phase segregation, Nat. Energy 5 (2020) 79–88, https://doi.org/10.1038/s41560-019-0535-7.

[48] B. Dong, J. Cui, Y. Gao, Y. Qi, F. Zhang, C. Li, Heterostructure of 1D Ta_3N_5 nanorod/$BaTaO_2N$ nanoparticle fabricated by a one-step ammonia thermal route for remarkably promoted solar hydrogen production, Adv. Mater. 31 (2019) 1808185, https://doi.org/10.1002/adma.201808185.

[49] Y. Tang, W. Zhou, Q. Shang, Y. Guo, H. Hu, Z. Li, Y. Zhang, L. Liu, H. Wang, X. Tan, T. Yu, J. Ye, Discerning the mechanism of expedited interfacial electron

transformation boosting photocatalytic hydrogen evolution by metallic 1T-WS2-induced photothermal effect, Appl. Catal. B Environ. 310 (2022), 121295, https://doi.org/10.1016/j.apcatb.2022.121295.